Chemical Synthesis of $Bi_{0.5}Sb_{1.5}Te_3$ Nanocrystals and Their Surface Oxidation Properties

Yixin Zhao and Clemens Burda*

Center for Chemical Dynamics and Nanomaterials Research, Department of Chemistry, Case Western Reserve University, 10900 Euclid Avenue, Cleveland, Ohio 44106

ABSTRACT Bismuth−antimony−telluride alloy, $Bi_{0.5}Sb_{1.5}Te_3$, nanocrystals (NCs) have been synthesized by direct chemical solution synthesis, in which the bismuth and antimony precursors, dissolved in a phenyl ether solution and coordinated with dodecanethiol, directly reacted with tellurium in trioctylphosphine. Transmission electron microscopy and X-ray diffraction (XRD) were used for the structure and morphology characterization of these NCs. Their XRD pattern evolution indicated that the reaction temperature plays a critical role in alloying and crystallization of $Bi_{0.5}Sb_{1.5}Te_3$ NCs. X-ray photoelectron spectrometry was used to study the alloy states and surface oxidation. It is found that the choice of the capping ligands can be important and useful in protecting against the surface oxidation of Bi_2Te_3-type thermoelectrical nanomaterials.

KEYWORDS: thermoelectric • Bi_2Te_3 • Sb_2Te_3 • $Bi_{0.5}Sb_{1.5}Te_3$ • nanocrystal • XRD • XPS

INTRODUCTION

Currently, applications of thermoelectrical (TE) materials are largely limited by low efficiencies compared to the more traditional energy conversion schemes. The TE energy conversion efficiency is directly related to the dimensionless figure of merit expressed by $ZT = S^2T\sigma/\kappa = S^2T/\kappa\rho$ (S = thermopower or Seebeck coefficient, T = temperature, σ = electrical conductivity, ρ = electrical resistivity, and κ = thermal conductivity) (1−4). However, recent theoretical and experimental studies have shown that nanostructured TE materials could have higher ZT values compared to the corresponding bulk materials (5−8). The promise of high ZT has inspired enthusiasm to develop different techniques to prepare nanostructured TE materials (9−17). The reported techniques included physical approaches such as ball milling and chemical approaches like chemical alloying (9), surfactant-directed synthesis (10), hydrothermal (11) and electrochemical deposition (12), and sonoelectrochemistry (13, 14). Bi_2Te_3 and Sb_2Te_3 are well-known room temperature TE materials. Nanostructured Bi_2Te_3 thin films have been prepared by electrochemical deposition (15, 16). Nanoscaled Bi_2Te_3 has been synthesized by surfactant-directed synthesis (10) and hydro/solvothermal and thermolysis reduction methods (11, 17). However, the hydro/solvothermal preparation needs high temperatures and high pressures, and the particle sizes of these prepared nanomaterials are relatively large. The solid solution of Bi_2Te_3 and Sb_2Te_3, $(Bi_xSb_{1-x})_2Te_3$, could increase the ZT value by reducing the thermal conductivity after alloying (6, 11). Here, we present the direct chemical synthesis of $Bi_{0.5}Sb_{1.5}Te_3$ nanocrystals (NCs) through a chemical ligand-based approach (18, 19) under mild conditions. The effect of the reaction time and temperature on the crystallization and alloying of $Bi_{0.5}Sb_{1.5}Te_3$ NCs and on the growth mechanism was investigated. In addition, the surface oxidation properties of these NCs are presented.

EXPERIMENTAL SECTION

Synthesis of Bi_2Te_3 and $Bi_{0.5}Sb_{1.5}Te_3$ NCs. ***Bi_2Te_3.*** A total of 0.6 mmol of bismuth acetate and 4 mL of dodecanethiol were dissolved in 20 mL of phenyl ether. The solution was then heated to different reaction temperatures for 60 min. The reaction flask was flushed with argon. A total of 1 mL of a 0.9 M trioctylphosphinetellurium (TOPTe) solution, which was freshly prepared by dissolving 0.9 mmol of tellurium powder (>99% pure) in 1 mL of TOP with moderate stirring for 12 h under the protection of argon, was injected into the reaction mixture, which was subsequently maintained at a constant reaction temperature for different times (5, 10, 30, and 60 min). The resulting black participate was washed and centrifuged with toluene, chloroform, and ethanol, respectively, and then dried under argon.

Sb_2Te_3. A total of 0.6 mmol of antimony chloride and 2 mL of dodecanethiol were dissolved in 20 mL of phenyl ether. The solution was then heated to different sets of reaction temperatures for 60 min. The reaction flask was flushed with argon. A total of 1 mL of a freshly prepared 0.9 M TOPTe solution was injected into the reaction mixture, which was subsequently maintained at a constant reaction temperature for different times (5, 10, 30, and 60 min). The resulting black participate was washed and centrifuged with toluene, chloroform, and ethanol, respectively, and then dried under argon.

$Bi_{0.5}Sb_{1.5}Te_3$. A total of 0.15 mmol of bismuth acetate, 0.45 mmol of antimony acetate, and 4 mL of dodecanethiol were dissolved in 20 mL of phenyl ether. This solution was then heated at different sets of reaction temperatures for 60 min. The reaction flask was flushed with argon, and then 1 mL of a freshly prepared 0.9 M TOPTe solution was injected into the reaction mixture, which was subsequently maintained at a constant reaction temperature for different times (5, 10, 30, and

* Tel: (+1)-216-368-5918. Fax: (+1)-216-368-3006. E-mail: burda@case.edu.
Received for review March 5, 2009 and accepted May 14, 2009

DOI: 10.1021/am900148d

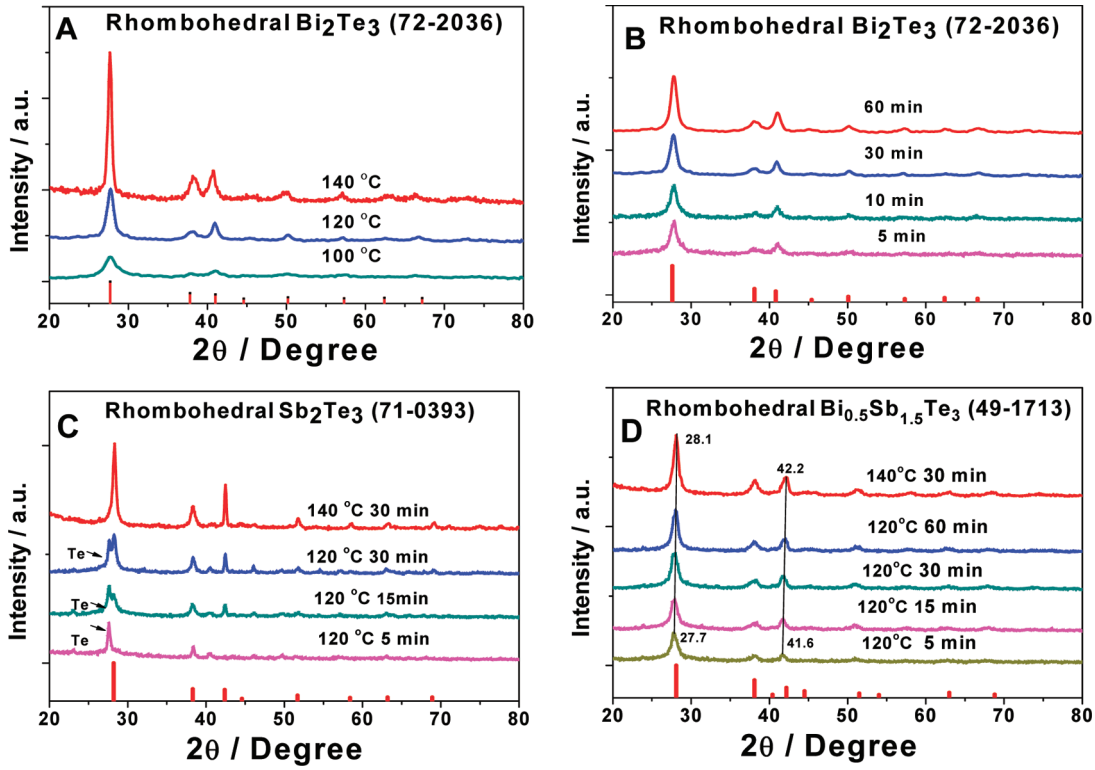

FIGURE 1. (A) XRD pattern evolution of Bi_2Te_3 NCs synthesized at different reaction temperatures for 30 min. The red bars are JCPDS standards for rhombohedral Bi_2Te_3 (72-2036). (B) XRD pattern evolution of Bi_2Te_3 NCs synthesized at 120 °C for different reaction times. The red bars are JCPDS standards for rhombohedral Bi_2Te_3 (72-2036). (C) XRD pattern evolution of Sb_2Te_3 NCs synthesized at different reaction temperatures and times. The red bars are JCPDS standards for rhombohedral Sb_2Te_3 (71-0393). (D) XRD pattern evolution of $Bi_{0.5}Sb_{1.5}Te_3$ NCs synthesized at different reaction temperatures and times. The red bars are JCPDS standards for rhombohedral $Bi_{0.5}Sb_{1.5}Te_3$ (49-1713).

60 min). The resulting black participate was washed and centrifuged with toluene, chloroform, and ethanol, respectively, and then dried under argon.

Characterization. The crystal structures of these NCs were examined with a Scintag X-1 Advanced powder X-ray diffractometer (2.4 °/min, Cu Kα radiation), and their morphology was characterized by using a transmission electron microscope, JEOL 1200CX (accelerating voltage = 80 kV). The binding energy and surface oxidation of the prepared NCs were explored on the X-ray photoelectron spectrometer (PHI 5600 XPS system).

RESULTS

X-ray Diffraction (XRD). The XRD patterns with broad peaks indicated that rhombohedral Bi_2Te_3, Sb_2Te_3, and $Bi_{0.5}Sb_{1.5}Te_3$ NCs were produced. The XRD pattern evolution of Bi_2Te_3 NCs in Figure 1A shows an increase of the peak intensity and a narrowing of the peaks of Bi_2Te_3 NCs with an increase of the reaction temperature for the same reaction time. From the XRD pattern evolution of Bi_2Te_3 NCs in Figure 1B, it can be found that Bi_2Te_3 NCs were formed very quickly almost at the start of the reaction. The XRD peaks became more intensive and narrower with an increase in the reaction time, which indicated that Bi_2Te_3 NCs became more crystallized and larger with time. Bi_2Te_3 NCs synthesized at 140 °C for 30 min in Figure 1A and Bi_2Te_3 NCs synthesized at 120 °C for 60 min in Figure 1B have very similar XRD patterns, which implies that the growth and crystallinity of Bi_2Te_3 NCs can be controlled by the reaction temperature or reaction time.

The XRD pattern evolution of Sb_2Te_3 NCs in Figure 1C also indicates that the crystallinity of these products is also related to the reaction temperature and time. Interestingly, a tellerium impurity was found at the 120 °C reaction. However, pure Sb_2Te_3 NCs, based on the XRD result, formed at the 140 °C reaction for 30 min. From the evolution of the XRD pattern of Sb_2Te_3 NCs in Figure 1C, the Sb_2Te_3 NCs formed relatively more slowly compared to the tellerium impurity at the 120 °C reaction. With an increase in the reaction time, the Sb_2Te_3 XRD peaks at 28.2° and 42.4° became more intense and narrower. On the other hand, the XRD intensity of the tellerium impurity, whose peaks are located at 27.6° and 40.4°, did not show significant variation. The results indicate that the reaction temperature plays an important role in the formation and crystallization of pure Sb_2Te_3 NCs.

The XRD pattern evolution of $Bi_{0.5}Sb_{1.5}Te_3$ NCs in Figure 1D shows that the alloying process is dependent on both the reaction temperature and time. When synthesized at 120 °C, the XRD peaks at 27.8° and 41.6°, corresponding to $(Bi_{0.5}Sb_{0.5})_2Te_3$, were already found at the beginning of the reaction and moved to 28.1° and 42.1°, the standard peak position for $Bi_{0.5}Sb_{1.5}Te_3$, and the peak intensity increased as the reaction progressed, which revealed that the (BiSb)Te_3 alloy crystal structure was formed and then more Sb_2Te_3 units alloyed into the alloy crystal lattice to form the final $Bi_{0.5}Sb_{1.5}Te_3$ crystal structure, as result of the alloying process. When the reaction was carried out at 140 °C for 30

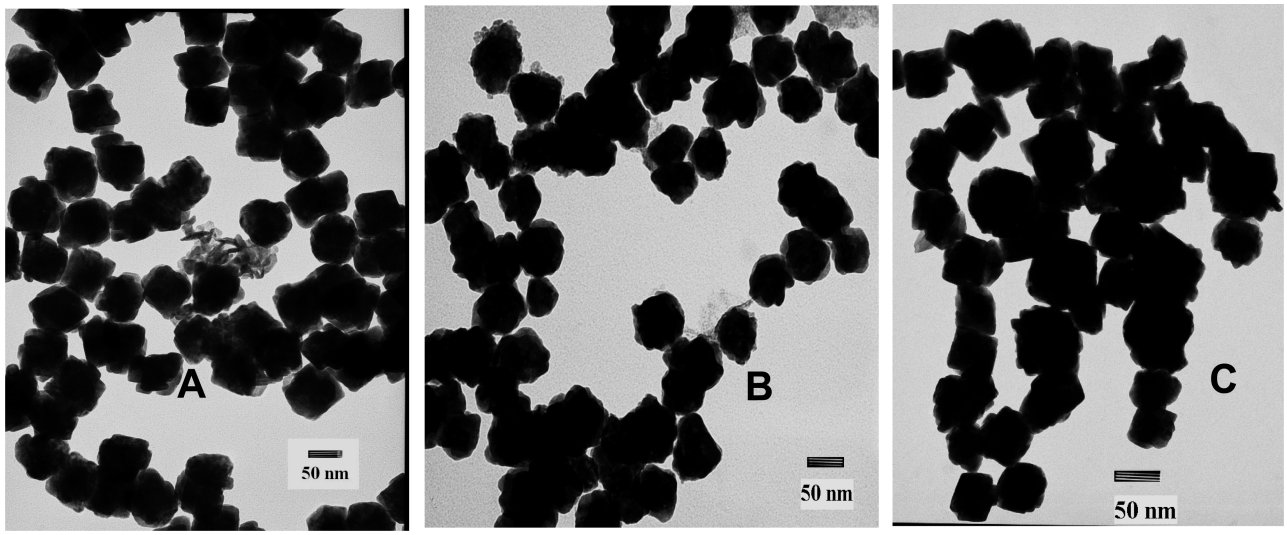

FIGURE 2. TEM micrographs of Bi_2Te_3 (A), Sb_2Te_3 (B), and $Bi_{0.5}Sb_{1.5}Te_3$ (C) NCs synthesized at 140 °C for 30 min.

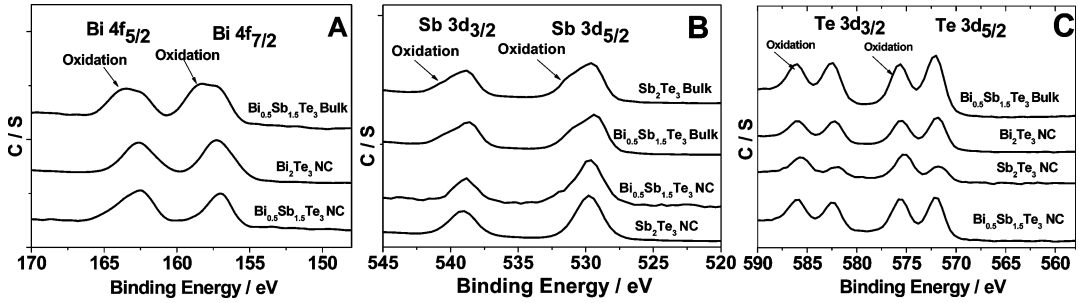

FIGURE 3. XPS for bismuth in $Bi_{0.5}Sb_{1.5}Te_3$ bulk, Bi_2Te_3 NCs, and $Bi_{0.5}Sb_{1.5}Te_3$ NCs (A), antimony in Sb_2Te_3 bulk $Bi_{0.5}Sb_{1.5}Te_3$ bulk, Sb_2Te_3 NCs, and $Bi_{0.5}Sb_{1.5}Te_3$ NCs (B); tellerium in $Bi_{0.5}Sb_{1.5}Te_3$ bulk, Bi_2Te_3 NCs, Sb_2Te_3 NCs, and $Bi_{0.5}Sb_{1.5}Te_3$ NCs (C). The measured graphs are arbitrarily offset for clarity.

min, the XRD pattern of the product showed relatively pure $Bi_{0.5}Sb_{1.5}Te_3$ peaks, which indicated that the reaction temperature also accelerated the alloying process for $Bi_{0.5}Sb_{1.5}Te_3$ alloy NCs.

Transmission Electron Microscopy (TEM). The TEM micrographs in Figure 2 show the morphology of these Bi_2Te_3, Sb_2Te_3, and $Bi_{0.5}Sb_{1.5}Te_3$ NCs. The particle sizes of these NCs are within a range of 40−80 nm. The particle shapes of these Bi_2Te_3, Sb_2Te_3, and $Bi_{0.5}Sb_{1.5}Te_3$ NCs are similar. For Bi_2Te_3 NCs (A), the particle sizes are 58.9 ± 7.8 nm. For Sb_2Te_3 NCs (B), the particle sizes are 49.4 ± 9.0 nm. For $Bi_{0.5}Sb_{1.5}Te_3$ NCs (C), the particle sizes are 43.6 ± 10.1 nm. The average sizes and size distributions were calculated by *Image J* software.

X-ray Photoelectron Spectrometry (XPS). The XPS results of Bi_2Te_3, Sb_2Te_3, and $Bi_{0.5}Sb_{1.5}Te_3$ NCs, which were synthesized at 140 °C for 30 min, are shown in Figure 3. The element stoichiometric ratios for Bi_2Te_3, Sb_2Te_3, and $Bi_{0.5}Sb_{1.5}Te_3$ are 39:61, 42:58, and 12: 31: 57, respectively, which are in reasonable agreement with the XRD stoichiometric assignments. The Bi $4f_{5/2}$ and $4f_{7/2}$ peaks located at around 162.6 and 157.2 eV indicated that there is no metallic Bi, and the alloying of Bi_2Te_3 and Sb_2Te_3 in $Bi_{0.5}Sb_{1.5}Te_3$ did not show significant changes in the binding energies of bismuth compared to the Bi_2Te_3 NC; just about a 0.2 eV shift was observed, which is less than the 0.4 eV energy resolution of the instrument. Also, the Bi $4f_{7/2}$ binding

Table 1. Bi $4f_{7/2}$ and Te $3d_{5/2}$ Oxidation Peak Percentages (%) in Bi_2Te_3 and $Bi_{0.5}Sb_{1.5}Te_3$ Bulk Material and Bi_2Te_3 and $Bi_{0.5}Sb_{1.5}Te_3$ NCs, Capped with Dodecanethiol or Oleic Acid, after Exposure to Air for 24 h[a]

	Bi $4f_{7/2}$/ 157.2 eV	Bi $4f_{7/2}$/ 158.5 eV (oxide)	Te $3d_{5/2}$/ 572.0 eV	Te $3d_{5/2}$/ 575.7 eV (oxide)
Bi_2Te_3 bulk	51	49	48	52
Bi_2Te_3 NCs	89	11	51	49
$Bi_{0.5}Sb_{1.5}Te_3$ bulk	58	42	55	44
$Bi_{0.5}Sb_{1.5}Te_3$ NCs (dodecanethiol)	92	8	57	43
$Bi_{0.5}Sb_{1.5}Te_3$ NCs (oleic acid)	82	12	69	31
$Bi_{0.5}Sb_{1.5}Te_3$bulk (fresh)[b]	*91*	*9*	*92*	*8*
	Sb $3d_{3/2}$/ 538.6 eV	Sb $3d_{3/2}$/ 540.2 eV (oxide)	Te $3d_{5/2}$/ 572.0 eV	Te $3d_{5/2}$/ 575.7 eV (oxide)
Sb_2Te_3 bulk	59	41	52	47
Sb_2Te_3 NCs (dodecanethiol)	90	10	56	44

[a] Also presented are Bi $4f_{7/2}$ and Te $3d_{5/2}$ oxidation peak percentages in freshly prepared $Bi_{0.5}Sb_{1.5}Te_3$ bulk material (italics) and Sb $3d_{3/2}$ and Te $3d_{5/2}$ oxidation peak percentages in bulk Sb_2Te_3 and Sb_2Te_3 NCs. The percentages were obtained by devolution of the XPS peak by *Multipak* software. [b] Freshly prepared $Bi_{0.5}Sb_{1.5}Te_3$ bulk ingot was just taken out of a vacuum-sealed tube and exposed to air for about 1 h during the XPS measurment sample preparation.

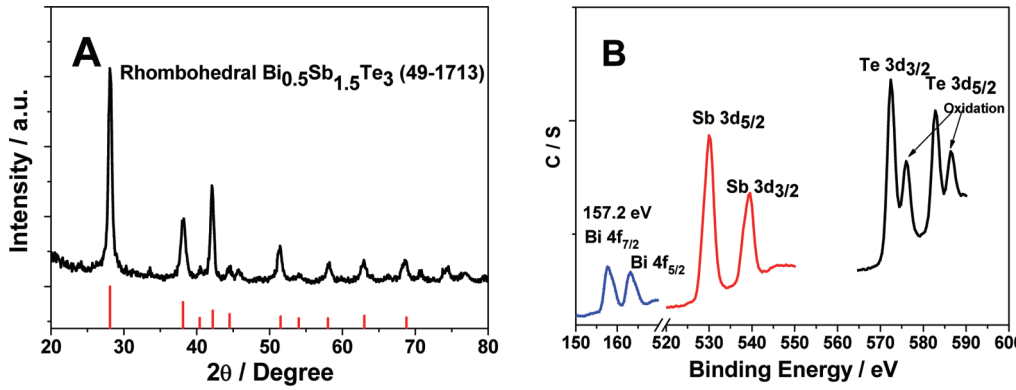

FIGURE 4. XRD for $Bi_{0.5}Sb_{1.5}Te_3$ NCs synthesized by using oleic acid (A). XPS peaks of bismuth, antimony, and tellerium in $Bi_{0.5}Sb_{1.5}Te_3$ NCs synthesized by using oleic acid (B).

of $Bi_{0.5}Sb_{1.5}Te_3$ shifted from 157.4 eV in bulk to 157.2 eV in NCs, as indicated in Figure 3A. The Bi $4f_{5/2}$ and $4f_{7/2}$ peaks have shoulders at higher binding energy, which indicates surface oxidation, as shown in Figure 3A,D. The Sb $3d_{5/2}$ and $3d_{3/2}$ peaks located at 529.2 and 538.4 eV suggest that there is no metallic Sb. The alloying of Bi_2Te_3 and Sb_2Te_3 in $Bi_{0.5}Sb_{1.5}Te_3$ did not significantly affect the binding energies of antimony. The Sb $3d_{5/2}$ and $3d_{3/2}$ peaks all have high-binding-energy shoulders, indicating surface oxidation, as shown in Figure 3B. However, the O 1s peak was also located at around 529.0 eV, and it will interfere with the Sb $3d_{5/2}$ signal for analysis, so the Sb $3d_{3/2}$ peak is more suitable than the Sb $3d_{5/2}$ peak for quantification. The Te $3d_{5/2}$ and $3d_{3/2}$ peaks were located at 572.0 and 582.3 eV, which indicated that there is no metallic tellerium impurity, which should appear at lower binding energy. In these samples, consistent with the XRD data, the tellerium shows almost the same binding energies in Bi_2Te_3, Sb_2Te_3, and their alloy $Bi_{0.5}Sb_{1.5}Te_3$ NCs. Oxidation peaks at 575.6 and 586.2 eV in Figure 3C show surface oxidation of Te atoms as pointed out previously (10, 20).

DISCUSSION

Crystal Structure and Growth Mechanism. The presence of tellerium impurity could be related to the growth mechanism of these NCs. The crystal growth mechanism of the CdTe (CdSe) NCs has been carefully studied by Alivisatos et al. (21) In their proposed mechanism, the cadmium precursors will first react with TOPTe (TOPSe) to form Cd−Te (Cd−Se) bonds and then cleave the TOP−Te (Se) bond to form CdTe/Se crystals during the ongoing reaction. We propose a similar growth mechanism for the Bi_2Te_3, Sb_2Te_3, and $Bi_{0.5}Sb_{1.5}Te_3$ NCs synthesized in this reaction. When M (M = Bi, Sb) precursors react with TOPTe, at first MTe or MTe_2 intermediates are formed, and these MTe and MTe_2 units crystallize to form the M_2Te_3 crystal structure at high temperature. If the reaction temperature is not high enough, the MTe or MTe_2 precursors slowly react with each other and form atomic Te, resulting in the measured tellerium impurity. The proposed mechanism suggests that the alloying process of the bismuth−antimony−telluride alloy, $(Bi_xSb_{1-x})_2Te_3$, depends on both the reaction temperature and time, which was confirmed by XRD evolution from $(Bi_{0.5}Sb_{0.5})_2Te_3$ to $Bi_{0.5}Sb_{1.5}Te_3$. However, the formation of the tellerium impurity is mainly dependent on the temperature. Also, the phase diagram of bulk $Bi_xSb_{2-x}Te_3$ shows that there will be a tellerium impurity at lower temperature (22, 23). The tellerium will also be formed at lower temperature for the bulk SbTe system when the Sb/Te ratio is near 2:3 (24). The reason that no tellerium impurity was found in Bi_2Te_3 and $Bi_{0.5}Sb_{1.5}Te_3$ NCs at low reaction temperature could come from their lower crystallization temperature compared to that of Sb_2Te_3. The melting point of bulk Sb_2Te_3 (617 °C) is higher than those of Bi_2Te_3 (586 °C) and $Bi_{0.5}Sb_{1.5}Te_3$ (605 °C) (23).

Surface Oxidation. Bando et al. have studied the surface oxidation process on bulk Bi_2Te_3 single crystals and found that a 2-nm-thick saturated oxide layer was formed on the surface upon exposure to an oxygen atmosphere for more than 24 h (20). The vacuum-prepared and stored bulk $Bi_{0.5}Sb_{1.5}Te_3$ ingot was also found to oxidize on its surface even upon exposure to air just during the XPS sample preparation process, as shown in Table 1. The oxidation of Bi_2Te_3-type TE materials deteriorates their electrical conductivity, and their TE figure of merit *ZT* will deteriorate as a result of that. The oxidation process could be an even more serious problem for nanostructured materials because of their high surface/volume ratio. However, Purkayastha's XPS data and our own XPS data show a disproportional oxidation extent for the bismuth and tellerium in these nanoparticles compared with Bando et al.'s bulk material. In the NC case, the XPS data of bismuth or antimony just had a small oxidation shoulder, while the tellerium showed a significant oxidation peak. In comparison, in the bulk Bi_2Te_3, the bismuth shows a similarly intense oxidation peak as tellerium. The surface oxidation percentages of bismuth and tellerium in the bulk Bi_2Te_3 and $Bi_{0.5}Sb_{1.5}Te_3$ ingot were found to be almost the same as those shown in Table 1. It is observed that the surface oxidation of bismuth is much lower than the oxidation of tellerium in the case of Bi_2Te_3 and $Bi_{0.5}Sb_{1.5}Te_3$ NCs. This phenomenon suggests that the oxidation of bismuth is slower than the oxidation of tellerium in these NCs. This may be due to protection from the surfactant-capping ligand dodecanethiol. To clarify this hypothesis, we have synthesized $Bi_{0.5}Sb_{1.5}Te_3$ NCs at 140 °C

for 30 min using oleic acid as the capping ligand instead of dodecanethiol. All other experimental parameters were kept identical. We observed XRD patterns similar to those shown in Figure 4A. The XPS in Figure 4B and surface oxidation percentages for bismuth and tellerium in Table 1 also showed that the tellerium oxidation percentage is much higher than the bismuth oxidation percentage, similarly to the $Bi_{0.5}Sb_{1.5}Te_3$ NCs capped with dodecanethiol. Moreover, dodecanethiol showed a stronger protection effect for bismuth against oxidation in the $Bi_{0.5}Sb_{1.5}Te_3$ NCs than oleic acid, which is a result of the higher binding affinity of the thiol group to bismuth compared to the carboxylic group. When the Bi $4f_{7/2}$ binding energies in Figures 3A and 4 are compared, it is found that the binding energies of $Bi_{0.5}Sb_{1.5}Te_3$ NCs capped by dodecanethiol have the lowest binding energy, or have the highest required oxidation potential, and that the $Bi_{0.5}Sb_{1.5}Te_3$ bulk material has the highest binding energy. This shows that the thermodynamics is not the cause for protection but rather a kinetic and steric hindrance.

CONCLUSION

Bismuth−antimony−telluride alloy $Bi_{0.5}Sb_{1.5}Te_3$ NCs have been successfully synthesized by direct chemical solution synthesis, by which the Bi_2Te_3 and Sb_2Te_3 NCs were also successfully synthesized. It is found that the reaction temperatures play an important role in the crystallization of Bi_2Te_3 and Sb_2Te_3 NCs and the alloying process of $Bi_{0.5}Sb_{1.5}Te_3$ NCs. The growth mechanism of the Bi_2Te_3, Sb_2Te_3, and $Bi_{0.5}Sb_{1.5}Te_3$ NCs is thought to be a stepwise cleavage and nucleation mechanism, similar to the mechanism proposed by Alivisatos et al. for CdSe(Te) quantum dots, and not an atomic precursor mechanism. The surface oxidation on these Bi_2Te_3, Sb_2Te_3, and $Bi_{0.5}Sb_{1.5}Te_3$ NCs shows a disproportional oxidation of the Bi/Sb atom compared to the Te atom, which is different from the bulk Bi_2Te_3 and $Bi_{0.5}Sb_{1.5}Te_3$. Therefore, the choice of the capping ligands can be critical to protecting against surface oxidation of Bi_2Te_3-type TE nanomaterials.

Acknowledgment. C.B. gratefully acknowledges financial support from the NSF (Grant CHE-0239688), NIRT (Grant 0608896), and ACS PRF (No. 45359-AC10).

REFERENCES AND NOTES

(1) DiSalvo, F. J. *Science* **1999**, *285*, 703–706.
(2) Nolas, G. S.; Sharp, J.; Goldsmid, H. J. *Thermoelectric Basic Principles and New Materials Developments*; Springer: Berlin, 2001; p 4.
(3) Service, R. F. *Science* **2004**, *306*, 806–807.
(4) Tritt, T. M.; Subramanian, M. A. *MRS Bull.* **2006**, *31*, 188–194.
(5) Dresselhaus, M. S.; Chen, G.; Tang, M. Y.; Yang, R. G.; Lee, H.; Wang, D. Z.; Ren, Z. F.; Fleurial, J. P.; Gogna, P. *Adv. Mater.* **2007**, *19*, 1043–1053.
(6) Poudel, B.; Hao, Q.; Ma, Y.; Lan, Y. C.; Minnich, A.; Yu, B.; Yan, X.; Wang, D. Z.; Muto, A.; Vashaee, D.; Chen, X. Y.; Liu, J. M.; Dresselhaus, M. S.; Chen, G.; Ren, Z. *Science* **2008**, *320*, 634–638.
(7) Ma, Y.; Hao, Q.; Poudel, B.; Lan, Y. C.; Yu, B.; Wang, D. Z.; Chen, G.; Ren, Z. F. *Nano Lett.* **2008**, *8*, 2580–2584.
(8) Snyder, G. J.; Toberer, E. S. *Nat. Mater.* **2008**, *7*, 105–114.
(9) Toprak, M.; Zhang, Y.; Muhammed, M. *Mater. Lett.* **2003**, *57*, 3976–3982.
(10) Purkayastha, A.; Yan, Q. Y.; Raghuveer, M. S.; Gandhi, D. D.; Li, H. F.; Liu, Z. W.; Ramanujan, R. V.; Borca-Tasciuc, T.; Ramanath, G. *Adv. Mater.* **2008**, *20*, 2679–2683.
(11) Xu, Y.; Ren, Z.; Ren, W.; Deng, K.; Zhong, Y. *Mater. Lett.* **2008**, *62*, 763.
(12) Lim, J. R.; Whitacre, J. F.; Fleurial, J. P.; Huang, C. K.; Ryan, M. A.; Myung, N. V. *Adv. Mater.* **2005**, *17*, 1488–1492.
(13) Qiu, X. F.; Lou, Y. B.; Samia, A. C. S.; Devadoss, A.; Burgess, J. D.; Dayal, S.; Burda, C. *Angew. Chem., Int. Ed.* **2005**, *44*, 5855–5857.
(14) Qiu, X. F.; Burda, C.; Fu, R. L.; Pu, L.; Chen, H. Y.; Zhu, J. J. *J. Am. Chem. Soc.* **2004**, *126*, 16276–16277.
(15) Li, S. H.; Toprak, M. S.; Soliman, H. M. A.; Zhou, J.; Muhammed, M.; Platzek, D.; Muller, E. *Chem. Mater.* **2006**, *18*, 3627–3633.
(16) Li, S. H.; Soliman, H. M. A.; Zhou, J.; Toprak, M. S.; Muhammed, M.; Platzek, D.; Ziolkowski, P.; Muller, E. *Chem. Mater.* **2008**, *20*, 4403–4410.
(17) Wang, W.; Lu, X. L.; Zhang, T.; Zhang, G. Q.; Jiang, W. J.; Li, X. G. *J. Am. Chem. Soc.* **2007**, *129*, 6702–6703.
(18) Urban, J. J.; Talapin, D. V.; Shevchenko, E. V.; Murray, C. B. *J. Am. Chem. Soc.* **2006**, *128*, 3248–3255.
(19) Lu, W. G.; Ding, Y.; Chen, Y. X.; Wang, Z. L.; Fang, J. Y. *J. Am. Chem. Soc.* **2005**, *127*, 10112–10116.
(20) Bando, H.; Koizumi, K.; Oikawa, Y.; Daikohara, K.; Kulbachinskii, V. A.; Ozaki, H. *J. Phys.: Condens. Matter* **2000**, *12*, 5607–5616.
(21) Liu, H. T.; Owen, J. S.; Alivisatos, A. P. *J. Am. Chem. Soc.* **2007**, *129*, 305–312.
(22) Abrikosov, N. K.; Poretskaya, L. V. *Inorg. Mater.* **1965**, *1*, 462–469.
(23) Caillat, T.; Carle, M.; Perrin, D.; Scherrer, H.; Scherrer, S. *J. Phys. Chem. Solids* **1992**, *53*, 227–232.
(24) Okamoto, H. *Desk Handbook: Phase Diagrams for Binary Alloys*; ASM International: Materials Park, OH, 2000; Vol. 1, p 1.

AM900148D